Time Correlation Between Different Forms of Energy Emitted from Rocks Under Compression

Giuseppe Lacidogna[1], Oscar Borla[1],Gianni Niccolini[2], Alberto Carpinteri[1]

[1]Politecnico di Torino, Department of Structural Engineering & Geotechnics,

Corso Duca degli Abruzzi 24 – 10129 Torino, Italy

[2]INRIM - National Institute of Metrological Research, Mechanics Division,

Strada delle Cacce, 91 – 10135 Torino, Italy

giuseppe.lacidogna@polito.it

Keywords: Compression**,** Brittle Failure, Acoustic Emission, Electromagnetic Emission, Neutron Measurements, Piezonuclear Reactions.

Abstract. It is possible to demonstrate experimentally that the failure phenomena, in particular when they occur in a brittle way, i.e. with a mechanical energy release, emit additional forms of energy related to the fundamental natural forces.

The authors have found experimental evidence and confirmation that energy emission of different forms occurs from solid-state fractures. The tests were carried out at the Laboratory of Fracture Mechanics of the Politecnico di Torino, Italy. By subjecting quasi-brittle materials such as granitic rocks to compression tests, it was observed for the first time bursts of neutron emission (NE) during the failure process, necessarily involving nuclear reactions, besides the well-known acoustic emission (AE), and the phenomenon of electromagnetic radiation (EME), which is highly suggestive of charge redistribution during material failure and at present under investigation.

In this work acoustic, electromagnetic and neutron emission were measured during new laboratory compression tests on rock specimens loaded up to failure. All the signals were acquired by a National Instruments Digitizer with eight channels simultaneously sampling. The aim was to find a time correlation between these three different forms of energy emissions from rocks under compression.

Tests were performed on magnetite and basalt specimens at constant displacement rate. AE signals were detected by applying to the specimen surface a piezoelectric (PZT) transducer with resonance frequency of about 150 kHz. EME signals were revealed by the induced current in a closed circuit due to change of the magnetic flux during specimen compression. The specimens were also monitored by means of He^3 proportional neutron detector.

During the tests were first detected AE signals, then EM emission. All the recorded signals were correlated with the load vs time diagrams. The EM signals were obtained, in particular, during the typical snap-back instabilities, which characterize the stress-strain curves of brittle materials such as rocks in compression. Neutron emission signals were generally identified at the end of the tests. As a matter of fact, neutron bursts usually occur when the behavior of the specimens in compression is particularly brittle or catastrophic.

Applications of these monitoring techniques to earthquake forecasting seem to be possible.

Introduction

It is possible to demonstrate experimentally that the brittle fracture in solid materials is accompanied by the release of different forms of energy.

By subjecting quasi-brittle materials such as granitic rocks to compression tests, it was observed for the first time bursts of neutron emission during the failure process [1-5], necessarily involving nuclear reactions, besides the well-known acoustic emission (AE) [6-13], and the phenomenon of electromagnetic radiation (EM) [14-19], which is highly suggestive of charge redistribution during material failure and at present under investigation.

The phenomenon of EME is regarded as an important precursor of critical phenomena in Geophysics, such as rocks fracture, volcanic eruptions and earthquakes [19,20]. For example, anomalous radiation of geo-electromagnetic waves observed before major earthquakes. At the laboratory scale, rocks and concrete under compression generate AE and EM emission nearly simultaneously. This evidence suggests that also EM emissions are generated during crack growth, reinforcing the idea that the EME phenomenon can be applied as a forecasting tool for earthquakes.

While the mechanism of AE is fully understood, being provided by transient elastic waves due to stress redistribution following fracture propagation [6-13], the origin of EME from fracture is not completely clear and different attempts have been made to explain it.

An explanation of the EME origin was related to dislocation phenomena [16], which however are not able to explain EME from fracture in brittle materials where the motion of dislocations can be neglected [17]. Frid et al. [17] and Rabinovitch et al. [11] recently proposed a model of the EME origin where, following the rupture of bonds during the cracks growth, mechanical and electrical equilibrium are broken at the fracture surfaces with creation of ions moving collectively as a surface wave on both faces. Lines of positive ions on both newly created faces (which maintain their charge neutrality unlike the capacitor model) oscillate collectively around their equilibrium positions in opposite phase to the negative ones. The resulting oscillating dipoles created on both faces of the propagating fracture act as the source of EME.

As regards the neutron emissions, in this work we present experimental tests performed on brittle rock test specimens (Magnetite and Basalt), using He^3 neutron device and bubble type BD thermodynamic neutron detectors.

For brittle specimens of larger dimensions, neutron emissions, detected by He^3, were found to be of about three orders of magnitude higher than the ordinary natural background level at the time of the catastrophic failure. These emissions fully confirm the previous tests [1-5] and are due to piezonuclear reactions, which depend on the different modalities of energy release during the tests. For specimens with sufficiently large size and slenderness, a relatively high energy release is expected, and hence a higher probability of neutron emissions at the time of failure.

The experimental analysis carried out by the authors may open a new possible scenario, in which the stress state of the elements firstly involves the generation of micro-cracks accompanied by mechanical energy release in the field of ultrasonic vibrations that can be measured using suitable AE equipments. Hence, the formation of coherent EM fields occurs over a wide range of frequencies, from few Hz to MHz. This excited state of the matter could be a precursor of subsequent resonance phenomena of nuclei able to produce neutron bursts in the presence of stress-drops or sudden catastrophic fractures.

Experimental set up

Experimental compression tests were performed on brittle rock test specimens under monotonic displacement control. The materials used for the tests are non-radioactive Magnetite and Basalt. In these tests 29 cylindrical specimens with different size and slenderness are used (Fig. 1). The compression tests were performed at the Fracture Mechanics Laboratory of the Politecnico di Torino. In Table 1, the experimental data concerning the tested specimens are summarized.

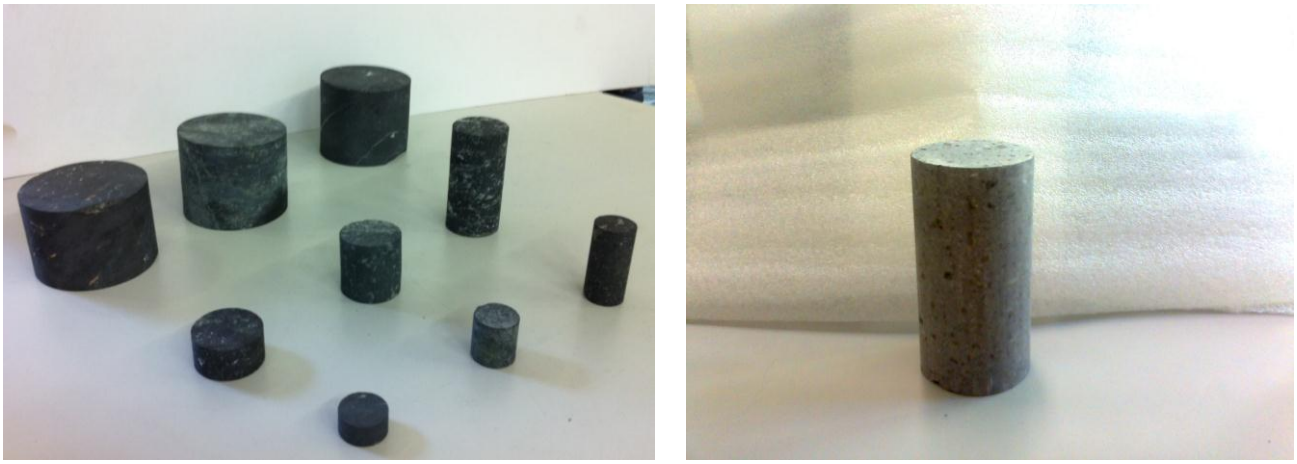

Figure 1: Magnetite (left) and Basalt (right) cylindrical specimens, by varying slenderness and size-scale.

All the specimens were subjected to uniaxial compression using a MTS servo-controlled hydraulic testing machine with a maximum capacity of 1000 kN. Each test was performed in piston travel displacement control by setting constant piston velocity. The specimens were arranged in contact with the press platens without any coupling materials, according to the testing modalities known as "test by means of rigid platens with friction".

The AE activity emerging from the compressed specimens was detected by attaching to the specimen surface a piezoelectric (PZT) transducer, resonant at about 150 kHz, which is able to convert the high-frequency surface movements due to the acoustic wave into an electric signal (the AE signal). Sensitivity of the transducer in the low-frequency range was measured by placing it on shaker excited with all frequencies in the range 0-10 kHz (white noise). The result of this calibration at low frequencies was 1.2 $\mu V/(mms^{-2})$. Resonant sensors are more sensitive than broadband sensors, which are characterized by a flat frequency response in their working range, and then they can be successfully used in monitoring of large-sized structures.

The EME detecting device, realized at the National Research Institute of Metrology (INRIM), is constituted by three pickup coils with different number of turns, made of a 0.2 mm copper wire, that are positioned around the monitored specimen. This instrumentation, which acquires data in the frequency range from few Hz up to 4 MHz, exploits the induction Faraday's law: the induced voltage in a closed circuit (loop) is proportional to the change of the magnetic flux throughout the circuit. The first coil, constituted by 5 turns, works in a frequency range from 300 kHz to 4 MHz. The other two coils constituted by 125 turns and 500 turns, work in the frequency range from few kHz to 20 kHz, and from few Hz to 1 kHz, respectively.

Due to the difficulties in neutron measurements in the presence of electromagnetic disturbances, EME measurement carries out both the validation of NE signals and the monitoring of EME from fracturing; the simultaneous presence of sharply peaked EME signals (well characterized and far from the continuous magnetic noise) and NE signals can be regarded as signature of ongoing damage process. As a further check on NE signals, a set of passive neutron detectors, based on the superheated bubble detection technique and insensitive to electromagnetic noise, were employed. A detailed description of the used neutron detectors is given.

Table 1. Tested specimens and their mechanical characteristics.

Specimens	Specimens Number	Dimension		Piston Velocity	Volume	Average Peak Load
		Diameter [mm]	Slenderness λ	[m/s]	[mm^3]	[kN]
Magnetite						
M-20-0.5	5	20	0.5	5E–7	3˙140	67.46
M-20-1	2	20	1	5E–7	6˙280	48.20
M-20-2	4	20	2	5E–7	12˙560	45.88
M-40-0.5	2	40	0.5	1E–6	25˙120	159.25
M-40-1	6	40	1	1E–6	50˙240	146.87
M-40-2	4	40	2	1E–6	100˙480	109.40
M-90-1	4	90	1	2E–6	572˙265	849.89
Basalt						
B-50-2	2	50	2	1E–6	196˙250	177.64

Specimens	AE		EME		NE	
	Average Frequency [Hz]	Average Highest Frequency [Hz]	Average Frequency [Hz]	Average Highest Frequency [Hz]	Average Neutron Background [10^{-2} cps]	Average Count Rate at the Neutron Emission [10^{-2} cps]
Magnetite						
M-20-0.5	20˙975	56˙990	19˙622	> 46˙000	4.84±1.21	Background
M-20-1	25˙889	49˙488	---	---	5.90±1.48	Background
M-20-2	23˙569	42˙984	32˙312	> 55˙000	5.70±1.42	Background
M-40-0.5	53˙354	133˙133	28˙278	> 49˙000	5.50±1.38	Background
M-40-1	60˙055	90˙997	37˙787	> 77˙000	5.06±1.26	18.75±4.69
M-40-2	33˙520	73˙385	35˙274	> 98˙000	5.60±1.40	25.96±6.49
M-90-1	52˙350	132˙062	110˙089	> 1 MHz	4.95±1.24	901.20±225.30
Basalt						
B-50-2	76˙668	165˙363	204˙417	> 335˙000	5.60±1.40	14.22±3.55

He^3 neutron proportional counter. The He^3 detector used in the compression tests under monotonic displacement control, and by ultrasonic vibration, is a He^3 type (Xeram, France) with electronics of preamplification, amplification, and discrimination directly connected to the detector tube. The detector is powered with 1.3 kV, supplied via a high voltage NIM (Nuclear Instrument Module). The logic output producing the TTL (transistor-transistor logic) pulses is connected to a NIM counter. The device was calibrated for the measurement of thermal neutrons; its sensitivity is 65 cps/$n_{thermal}$ (± 10% declared by the factory) i.e., a thermal neutron flux of 1 thermal neutron/s cm^2 corresponds to a count rate of 65 cps.

Considering that the fracture of dielectric materials, such as rocks, can lead to the emission of charged and neutral particles (electrons, photons, hard X-rays), in order to avoid possible false neutron measurements the output of the detector is enabled for detecting signals only exceeding a

fixed amplitude. This threshold value was determined by measuring the analog signal of the detector by means of a Co-60 gamma source (half-life: 5.271 years, type decay: beta$^-$, beta maximum energy: 317.8 keV, gammas: 1173.2 keV and 1332.5 keV). The presence of an interfering capacity on the charge preamplifier input increases the electronic noise and consequently the probability of spurious counts. For this reason, the coaxial cable used for connecting detector and charge preamplifier presented a low capacity (36 pF/m) and a short length (about 50 cm). Moreover, during the experimental measurements, the front-end electronics was screened with aluminum foils, and the He^3 tube was immersed in a sound-absorbing substance such as polystyrene in order to avoid possible accidental impacts and vibrations.

Neutron bubble detectors. A set of passive neutron detectors insensitive to electromagnetic noise and with zero gamma sensitivity was used in compression tests under cyclic loading. The dosimeters, based on superheated bubble detectors (BTI, Ontario, Canada) (Bubble Technology Industries (1992)) [22], are calibrated at the factory against an Am-Be source in terms of NCRP38 (NCRP report 38 (1971)) [23]. Bubble detectors provide instant visible detection and measurement of neutron dose. Each detector is composed of a polycarbonate vial filled with elastic tissue-equivalent polymer, in which droplets of a superheated gas (Freon) are dispersed. When a neutron strikes a droplet, the latter immediately vaporizes, forming a visible gas bubble trapped in the gel. The number of droplets provides a direct measurement of the equivalent neutron dose. These detectors are suitable for neutron integral dose measurements, in the energy ranges of thermal neutrons (E = 0,025eV) and fast neutrons (E > 100 keV).
All the signals (AE, EME and NE) were acquired by a National Instruments Digitizer with eight channels simultaneously sampling at 1 MSa/s. The trigger was set to the AE channel with a detection threshold fixed at 20 mV to filter out the background noise. For all the specimens, the recorded AE, EME and NE time series were related to the time history of the applied load.

Test results

AE and EME measurements. In this work the experimental results of four specimens (3 of Magnetite and 1 of Basalt) are examined in detail. All specimens were tested in compression up to failure, showing a brittle response with a rapid decrease in load-carrying capacity when deformed beyond the peak load (Figs. 2 and 3). Experimental evidence indicates the presence of AE, EME and NE activity. It is interesting to note that in this experimental campaign –unlike of those carried out by the authors on specimens of other materials, such as concrete, Luserna stone, Carrara marble and Syracuse limestone [14,15]– the EME activity is much more widespread during the loading process, and not just concentrated at the moment of the final collapse.
As a matter of fact, in the Magnetite specimen P1 (M-40-1 type), which behaviour is described by the load vs. time curve of Fig. 2 (left), the observed bursts of AE and EME activity can be clearly correlated with the stress drops occurred before the moment of the collapse, Fig. 2 (upper and middle left). In the Magnetite specimen P2 (M-90-1 type), characterized by a perfectly brittle behaviour without evident stress drops before the final collapse (note the linearity till failure of the load vs. time curve in Fig. 2 (right)), the specimen failure was preceded by two closely correlated bursts of AE and EME activity at nearly 80% of the peak load, Fig. 2 (upper and middle right). This activity, particularly as regards electromagnetic emission, can be due to the behaviour under loading of Magnetite rocks that –being rich in iron, about 65% in weight– determines the formation of magnetic charges generated by friction during the loading process, and their spontaneous release independently from the formation of macro-cracks at the time of final collapse.
As a particular case, the load vs. time curve of the Magnetite specimen P3 (M-20-1 type) is double-peaked with a significant stress drop at about 60% of the test duration, followed by a drop in the AE

rate, Fig. 3 (left). This momentary relaxation in the AE activity describes the well-known Kaiser effect [24], which states that, after stress drops, AE activity is very low during the reloading of the material until the stress exceeds the previous reached values, Fig. 3 (upper left). This relaxation was observed also in the EME activity, Fig. 3 (middle left), confirming the close correlation degree between these two phenomena.

NE measurements. As regards the NE measurements, the He^3 neutron detector was switched on at least one hour before the beginning of each compression test, in order to reach the thermal equilibrium of electronics, and to make sure that the behaviour of the device was stable with respect to intrinsic thermal effects. For the considered specimens P1, P2 and P3 the average measured background level ranges from $(4.00\pm1.00)\cdot10^{-2}$ to $(6.40\pm1.60)\cdot10^{-2}$ cps. In general, neutron measurements of specimens M-20-1 type yielded value comparable with the ordinary natural background, whereas in specimens M-40-1 type the experimental data exceeded the background value by about four times. For specimens M-90-1 type the neutron emissions achieved values up to three orders of magnitude higher than the ordinary background.
In Figs. 2 and 3 (left) the load vs. time diagram, and the neutron count rate evolution for each specimen are shown. Moreover bursts of NE activity were observed at the failure time of specimens P1 (M-40-1 type) and P2 (M-90-1 type), Fig. 2 (lower), confirming the need of catastrophic ruptures, i.e., characterized by sudden release of the stored strain energy, to obtain such anomalous neutron emissions.
Furthermore, during the compression tests a rise of the thermal equivalent neutron dose, analysed by neutron bubble detectors, consistently with the increment of the neutron level measured by the He^3 device, was observed. In particular for the specimen P2 (M-90-1 type), a value of more than 1000 times higher with respect to the ordinary background was found at the end of the test.

AE, EME and NE time correlation. Test results on the Basalt specimen P4 (B-50-2 type) as well gives a high degree of correlation among the three emissions time series and the load time history. As an example, considering a time window of 0.6 s starting from the 1921.7 s by the beginning of the test, AE bursts followed by an EME pulse in the kHz frequency gap are shown in Fig. 3 (right). Similar simultaneous EM pulses have been observed in the Hz and MHz range that, for reasons of space, are not included in figure. The time window is related to the evident stress drop indicated by a circle in the load vs. time diagram, Fig.3 (right).
As already discussed in [14], AE and EME signals, from a growing fracture, follow a time delay consistent with their propagation velocities. Being d the distance source fracture-AE transducer, v_{AE} and v_{EME} the average propagation velocities of AE and EME waves with $v_{AE} << v_{EME}$, the time delay can be estimated by $\Delta t = d/ v_{AE}$. Inserting $d = 10^{-1}$ m and $v_{AE} = 10^3$ m s^{-1}, an estimation of the time delay for the considered event is $\Delta t = 10^{-4}$ s = 100 μs.
If then we consider that the main crack propagation, in the specified time-window, takes place (begins its first motion) when the first AE peak of great amplitude is recorded, the main EME pulse follows the AE burst also considering the different average propagation velocities of AE and EME signals. Therefore, the EME signal seems to spread during the mechanical vibration generated by the fracture. Finally, the NE event is observed at the time of catastrophic failure of the specimen, Fig. 3 (upper and lower right).

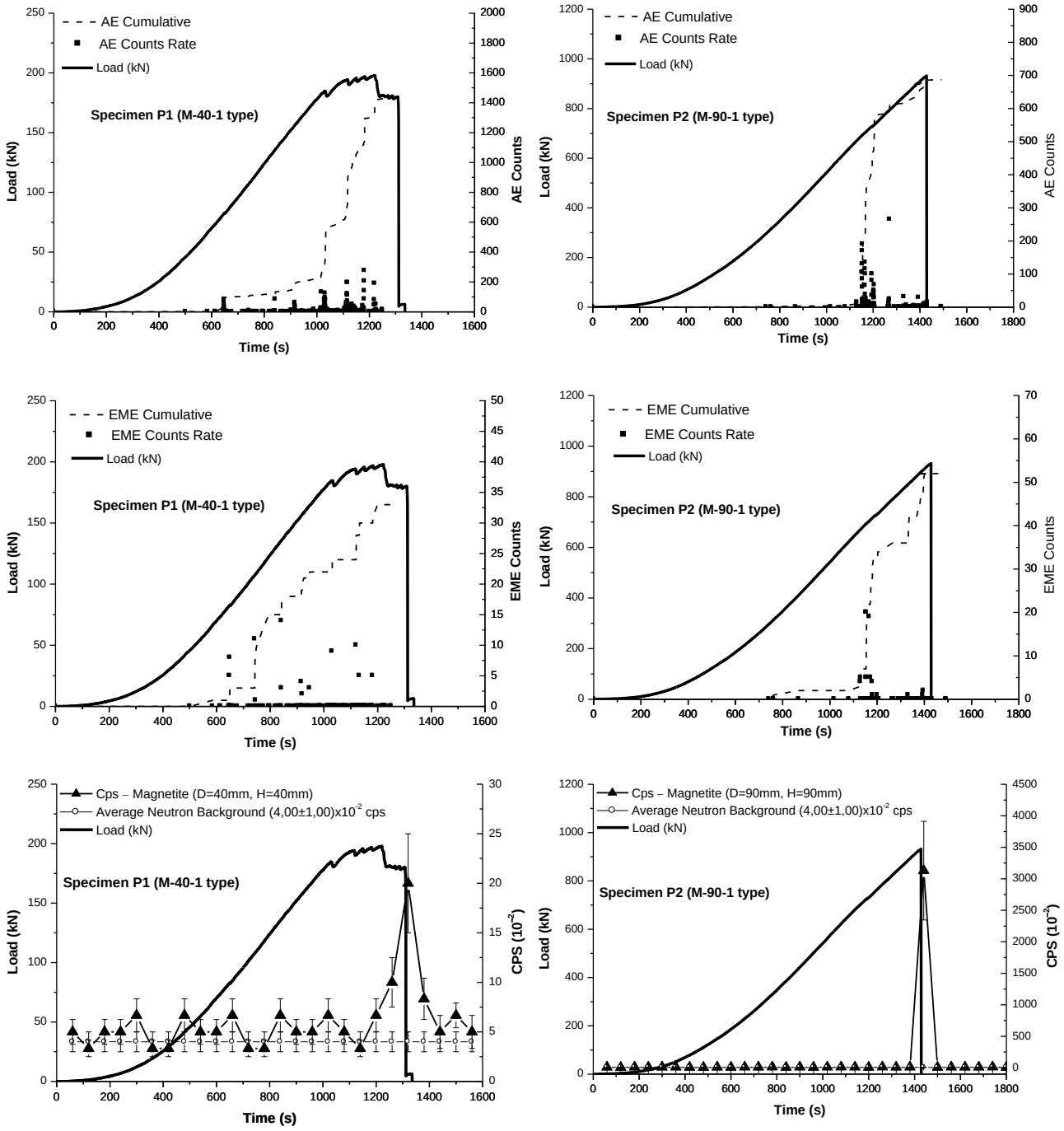

Figure 2: Load vs. time curve of the Magnetite specimen P1 (M-40-1 type) (left); accumulated number and rate of AE (upper left); accumulated number and rate of EME (middle left); NE count rate (lower left). Load vs. time curve of the Magnetite specimen P2 (M-90-1 type) (right); accumulated number and rate of AE (upper right); accumulated number and rate of EME (middle right); NE count rate (lower right).

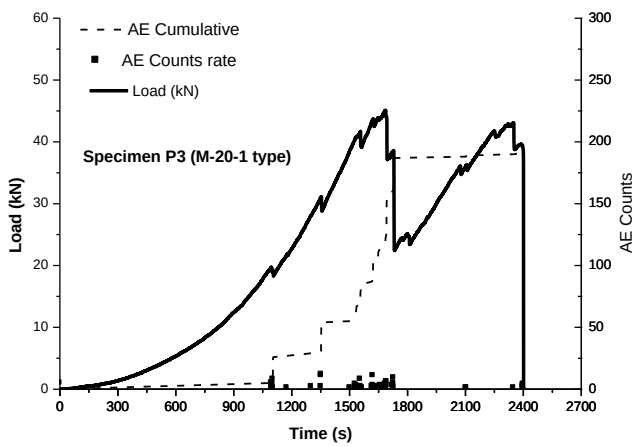

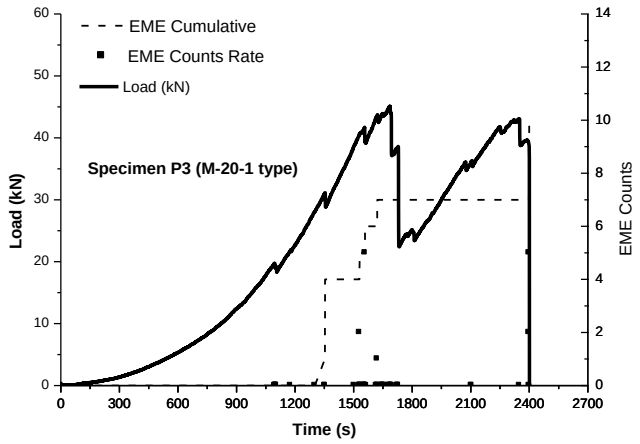

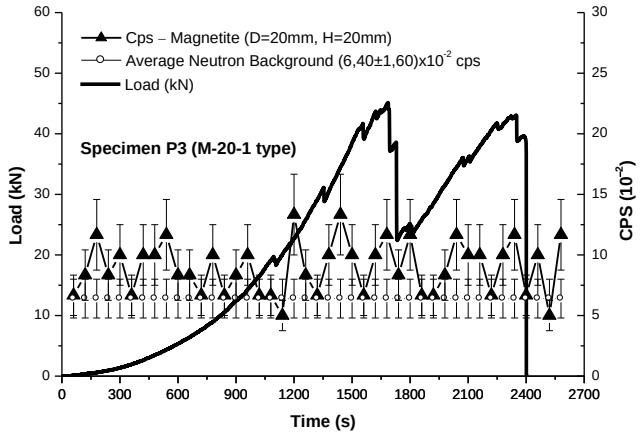

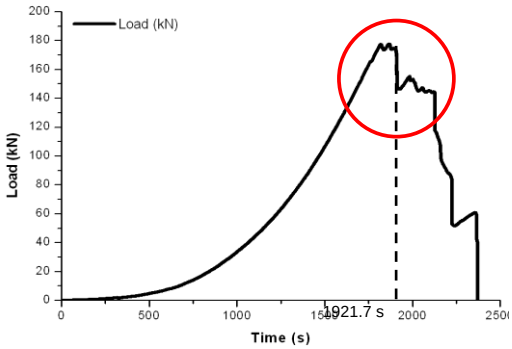

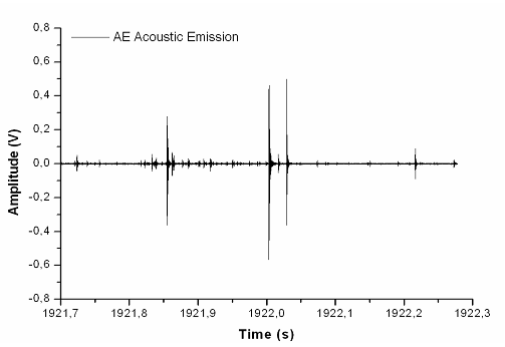

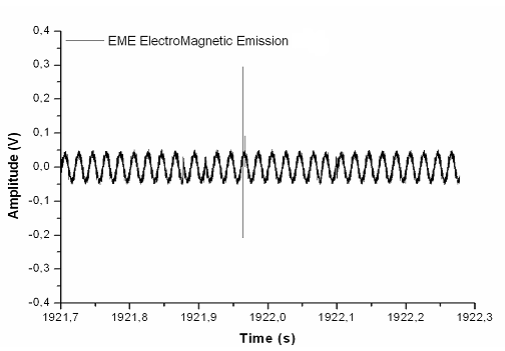

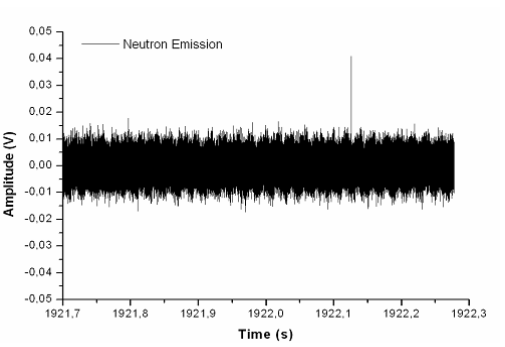

Figure 3: Load vs. time curve of the Magnetite specimen P3 (M-20-1 type) (left); accumulated number and rate of AE (upper left); accumulated number and rate of EME (middle left); NE count rate (lower left). Load vs. time curve of the Basalt specimen (upper right); AE, EME (middle right) and NE signals (lower right) detected in a time window of 0.6 s, starting from 1921.7 s by the beginning of the test.

Conclusions

The experimental evidence presented in this paper confirms the simultaneous investigation of AE and EME signals as collapse precursors in natural materials like rocks. The observed EME were strictly correlated in time with AE signals in all the tested specimens. Bursts of AE and EME activity were observed when significant stress drops occur. This suggests the use of electromagnetic measurements to enhance monitoring systems based on the AE technique. Bursts of NE activity were observed only when specimen fails in a sudden, catastrophic way. In particular, for specimens with sufficiently large size, the neutron flux was found to be of about three orders of magnitude higher than the background level at the time of catastrophic failure. Therefore, the observed acoustic, electromagnetic, and neutron activity from laboratory experiments looks promising for effective applications also at the geophysical scale.

The results obtained from this analysis show how the crack generation is accompanied by mechanical energy release in the field of ultrasonic vibrations detected by AE sensors. It was also observed that, considering specimens with the same shape, the AE signals reach high frequency peaks for low slenderness, whereas the EME frequencies increase with the samples size.

The higher neutron emissions took place for specimens with EME detected in the field of MHz. This shows that the formation of coherent EM fields occurs over a wide range of frequencies, from kHz to MHz, during the fracture propagation. This excited state of the material could be a precursor of subsequent resonance phenomena in condensed matter.

Acknowledgments

The financial support provided by the Piedmont Region (Italy) to the Project ‘‘Preservation, Safeguard and Valorisation of Masonry Decorations in the Architectural Historical Heritage of Piedmont” (RE-FRESCOS) is gratefully acknowledged. Special thanks are also due to Mr. F. Argiolas for the providing of the magnetite specimens.

References

[1] A. Carpinteri, F. Cardone and G. Lacidogna. Strain, Vol. 45, (2009), pp. 332-339.
[2] F. Cardone, A. Carpinteri and G. Lacidogna. Physics Letters A, Vol. 373, (2009), pp. 4158-4163.
[3] A. Carpinteri, F. Cardone and G. Lacidogna. Experimental Mechanics, Vol. 50, (2010), pp. 1235-1243.
[4] A. Carpinteri, O. Borla, G. Lacidogna and A. Manuello. Physical Mesomechanics, Vol. 13, (2010), pp. 268-274.
[5] A. Carpinteri, G. Lacidogna, A. Manuello and O. Borla. Strenght Fracture and Complexity, Vol. 7, (2011), pp. 13-31.
[6] K. Mogi. Bull. of Earthquake Res. Inst., Vol. 40, (1962), pp. 125-173.
[7] D. Lockner. Int. J. Rock Mech. Min. Sci. Geomech. Abs., Vol. 7, (1993), pp. 883–889.
[8] M. Ohtsu. Magazine of Concrete Research, Vol. 48, (1996), pp. 321–330.
[9] J. B. Rundle, D. L. Turcotte, R. Shcherbakov, W. Klein and C. Sammis. Reviews of Geophysics, Vol. 41, (2003), pp. 1-30.
[10] G. Niccolini, A. Schiavi, P. Tarizzo, A. Carpinteri, G. Lacidogna, A. Manuello. Physical Review E, Vol. 82, (2010), pp. 46115/1-46115/5.
[11] A. Carpinteri, and G. Lacidogna. Materials and Structures, Vol. 39, (2006), pp. 161-167.
[12] A. Carpinteri and G. Lacidogna. Journal of Structural Engineering (ASCE), Vol. 132, (2006), pp. 1681-1690.
[13] A. Carpinteri and G. Lacidogna. Engineering Structures, Vol. 29, (2007), pp. 1569-1579.
[14] G. Lacidogna, A. Carpinteri, A. Manuello, G. Durin, G. Niccolini, and A. Agosto. Strain, Vol. 47 Suppl. 2, (2010), pp. 144-152.

[15] A. Carpinteri, G. Lacidogna, A. Manuello, G. Niccolini, A. Schiavi and A. Agosto. Experimental Techniques, doi: 10.1111/j.1747-1567.2011.00709.x, 1-12, 2010
[16] A. Misra. Physics Letters A, Vol. 62, (1977), pp. 234-236.
[17] V. Frid, A. Rabinovitch and D. Bahat. J. Phys. D., Vol. 36, (2003), pp. 1620-1628.
[18] V. Hadjicontis, C. Mavromatou and D. Nonos. Nat. Hazards and Earth System Science, Vol. 4, (2004), pp. 633-639.
[19] J. W. Warwick, C. Stoker, and T. R. Meyer. J. Geophys. Res., Vol. 87, (1982), pp. 2851-2859.
[20] T. Nagao, Y. Enomoto, Y.Fujinawa, et al. Journal of Geodynamics, Vol. 33, (2002), pp. 401-411.
[21] A. Rabinovitch, V. Frid and D. Bahat. Tectonophysics, Vol. 431, (2007), pp. 15-21.
[22] Bubble Technology Industries. Instruction manual for the Bubble detector, Chalk River, Ontario, Canada, 1992.
[23] National Council on Radiation Protection and Measurements. Protection Against Neutron Radiation, NCRP Report 38, 1971.
[24] J. Kaiser. Ph. D. dissertation, Munich (FRG), Technische Hochschule München, 1950.